LYAKHOVSKY, V., ILCHEV, A., and AGNON, A. Modelling of damage and instabilities in rock mass by means of a non-linear rheological model. *Rockbursts and Seismicity in Mines—RaSiM5*. South African Institute of Mining and Metallurgy, 2001.

Modelling of damage and instabilities in rock mass by means of a non-linear rheological model

V. LYAKHOVSKY*, A. ILCHEV†, and A. AGNON‡

**Geological Survey of Israel, Jerusalem, Israel*

†ISS International Limited, Welkom, South Africa

‡The Institute of Earth Sciences, The Hebrew University of Jerusalem, Givat Ram, Jerusalem, Israel

Introduction

Fracture processes control the mechanical response and stability of rock mass under variable loading. We present here a damage mechanics approach based on the assumption that the density of micro cracks is uniform over a length scale much larger than the length of a typical crack, yet much smaller than the linear size of the volume considered. In a specimen deformed in a rock-mechanics experiment, micro crack density can be measured over a sub-centimetre scale where it is considered as distributed damage. On the other hand, at length scales typical for the mining environment, individual faults shorter than, say, one metre can be considered as distributed damage. For any system with a sufficiently large number of cracks, one can define a representative volume in which the crack density is uniform. An intensive damage variable can be introduced for a representative volume, which includes numerous small cracks. Following Kachanov[1] the damage variable is related to the reduction of the rigidity of a spatial domain relative to the modulus of an ideal crack-free solid. The present damage rheology model Lyakhovsky *et al.*[2,3] treats two aspects of the physics of damage: (1) A mechanical aspect, namely the sensitivity of the macroscopic elastic shear modulus to distributed cracks and to the sense of loading, and (2) a kinetic aspect, namely the evolution of damage (degradation–recovery of elasticity) in response to loading. For an intuitive understanding of the former, consider the response of a single crack. Across the crack there is no cohesion, so under extension perpendicular to the plane of the crack it dilates, displaying diminished resistance to loading. Compression, on the other hand, is resisted by contact forces across the crack. Hence distributed cracks modify the elastic behaviour by breaking the symmetry to loading-unloading and reducing the apparent moduli. In addition to this mechanical aspect of distributed cracks, irreversible sliding on microcracks gives rise to a kinetic aspect. Sliding takes place on micro cracks if the stresses on them exceed the static friction limit. Under Coulomb friction, the critical stress for sliding is proportional to the normal stress (Byerlee[4]). We replace the Coulomb stress criterion constrained by experiments on undamaged media with an equivalent critical applied strain, which does not depend on the effective modulus. For a general three-dimensional loading it is convenient to define the critical strain in terms of the invariants of the strain tensor [Lyakhovsky *et al.*[2]]. The first invariant, $I_1=\varepsilon_1+\varepsilon_2+\varepsilon_3$, representing dilation, is independent of shear, whereas the second invariant, $I_2 = \varepsilon_1^2+\varepsilon_2^2+\varepsilon_3^2$, depends on shear as well as on dilation (ε_1, ε_2, ε_3 are principal elastic strains). Therefore the ratio $\xi=I_1/\sqrt{I_2}$ can be mapped to the coefficient of friction (Agnon and Lyakhovsky[5]; Lyakhovsky *et al.*[2]). The connection of the friction law to damage kinectics lies in the competition between degradation and healing. If a micro crack is loaded beyond the friction limit the crack surfaces slide past each other, loading the tips and creating more damage. Hence the rate of damage change is positive. Below the friction limit, healing processes are active and the damage rate is negative.

We briefly list below some indications of distributed damage in natural rocks and rock samples which form the experimental basis for our theoretical damage approach. Then, we present the main equations of the damage rheology model and numerical scheme for three-dimentional simulations. Finally, we discuss two examples of simplified simulations demonstrating the ability of damage rheology and the accuracy of numerical calculations.

Distributed damage in rocks

Pioneering studies of fractures and faults treated the crust as an infinite, perfectly elastic medium, e.g., Anderson[6]. Subsequent studies accounted for the finite length of faults, and the perturbation to the regional stress field due to the proximity of additional faults, see Chinnery[7]. Field mapping often shows that the density of faults depends on the scale of the map, so higher resolution increases the number of faults in a given domain [Scholz[8]]. This complexity limits the use of methods that specify the positions of isolated cracks in the deforming region. Some field observations suggest that the size of the damage zone (or process zone) grows with the size of the fracture, in violation of the premises of the critical stress intensity factor approach [Rubin[9,10]]. This is decisively documented around dykes that form by the injection of magma into fractures [Delaney *et al.*[11], Baer[12], Weinberger *et al.*[13], Hoek[14]]. The strain components are dimensionless and it is therefore not possible to introduce scaling, except for linear relations between fracture lengths and displacements (Scholz *et al.*[15]). Such scaling is compatible with field observations that suggest the size of the process zone grows proportionally to the fracture length (Vermilye and Scholz[16]). However, the general applicability of the universal scaling remains the subject of some debate. The length of the process zone around the tip of a propagating fracture, as well as the fracture energy and toughness, are functions of the specimen (or structure) size and shape, e.g.,

Bazant and Kazemi[17]. Sinclair and Chambers[18] have reviewed the experimental evidence of the size effect. Field observations of two populations of tensile fractures in the Krafla fissure swarm of north-east Iceland clearly show breaking of self-similarity and non-universal scaling of fracture length and aperture (Hatton *et al.*[19], Renshaw and Park[20]). Seismic events that occur close to underground excavations in a complex geological setting are often associated with many zones of permanent deformation, where width is not necessarily scaled linearly to the length or amount of slip.

The damage in the form of microcracks profoundly affects rock strength and rock elastic parameters (Nishihara[21], Zoback and Byerlee[22], Schock[23], Schock and Louis[24], Lockner and Byerlee[25], Alm *et al.*[26], Reches and Lockner[27], Weinberger *et al.*[28], Pestman and Munster[29]) and leads to vanishing elastic moduli at large stresses just before failure, e.g., Lockner and Byerlee[25], Lockner *et al.*[30]. The investigations of fracturing of rocks by Yukutake[31], Lockner *et al.*[32] and Reches and Lockner[27] show that this process can not be described in terms of single-crack propagation. While linear elastic fracture mechanics (LEFM) assumes the size of the inelastic zone at the crack tip to be negligibly small, the experiments show that this zone has a significant size. The finite size effect of the fracture process zone is often treated with models which specify a cohesive zone near the crack tip within the plane of the crack (Dugdale[33], Barenblatt[34,35], Ida[36], Palmer and Rice[37], Rubin[38], Willemse and Pollard[39]). This approach is useful when the crack geometry is well defined, and in contrast to LEFM the cohesion zone models do not contain an unphysical crack-tip singularity. In most engineering and rock-like materials a slowly propagating crack is preceded by an evolving damage zone distributed around its tip, e.g., Bazant and Cedolin[40], Lockner *et al.*[32], and, hence, controls the macro-crack trajectory and the growth rate (Huang *et al.*[41], Chai[42], Zietlow and Labuz[43]). Thus it is desirable to account explicitly for the distribution of damage in simulations of fault evolution.

Damage rheology model

In this section, the main features of the damage rheology model are presented. Detailed explanations and comparisons with rock mechanics experiments may be found in Lyakhovsky *et al.*[2,3].

The cumulative effect of distributed micro-cracks and flaws in the elastic material leads to non-linearity, which is described by an energy potential equation of the form:

$$U = \frac{1}{\rho}\left(\frac{\lambda}{2} I_1^2 + \mu I_2 - \gamma I_1 \sqrt{I_2}\right), \qquad [1]$$

where ρ is the density: $I_1 = \varepsilon_{ii}$, $I_2 = \varepsilon_{ij}$ (summation over repeated indices is understood) are two invariants of the strain tensor ε_{ij}; and λ, μ and γ are Lame coefficients. The energy expression [1] includes a new non-analytical, second-order term, in addition to the quadratic terms containing invariants of the strain tensor of the Hookean elastic solid. The effect of variable damage is introduced by making the Lame coefficients functions of the damage level α, (i.e., $\lambda(\alpha)$, $\mu(\alpha)$ and the coupling coefficient $\gamma(\alpha)$; $0 \le \alpha \le 1$). The variable α can be envisaged as the density of microcracks in a laboratory specimen, or as the density of small faults in a crustal domain. In damage-free material ($\alpha=0$), the coupling coefficient γ vanishes and the Hookean energy potential is retrieved. The coefficient γ increases with material degradation and achieves its maximum for the totally destroyed material ($\alpha=1$). Following Murnaghan[44], the stress tensor, σ_{ij}, is defined as the derivative of the energy potential (1) with respect to the strain tensor

$$\sigma_{ij} = \rho \frac{\partial U}{\partial \varepsilon_{ij}} = \left(\lambda - \frac{\gamma}{\xi}\right) I_1 \delta_{ij} + 2\left(\mu - \frac{1}{2}\gamma\xi\right)\varepsilon_{ij} \qquad [2]$$

The non-zero coupling coefficient γ makes the effective elastic moduli dependent on the strain diagonality, $\xi = I_1/\sqrt{I_2}$, which varies from $-\sqrt{3}$ for 3-D compaction to $\sqrt{3}$ for 3-D dilation. $\xi = \pm 1$ means uniaxial tension or compression respectively, and $\xi=0$—pure shear under zero volumetric strain ($I_1=0$).

The amount of damage evolves in time as a result of the applied loads. Using the balance equations of the energy and entropy, and accounting for irreversible changes related to viscous deformation and material damage, the equation of damage evolution has the form (Lyakhovsky *et al.*[2]).

$$\frac{d\alpha}{dt} = -C\frac{\partial U}{\partial \alpha} \qquad [3]$$

where C is a positive function of the state variables describing the temporal rate of the damage process. It must be emphasized that this approach describes not only damage increase, but also a process of material recovery associated with healing of micro-cracks, which is favoured by high confining pressure, low shear stress, and especially under high temperature. Agnon and Lyakhovsky[5] chose that the moduli μ and γ be linear functions of α (i.e., $\mu = \mu_0 - \alpha_r$, $\gamma = \alpha\gamma_r$) and the modulus λ be constant. The values of μ_r, γ_r are calculated from the condition of material destruction for $\alpha=1$ (Equation [15] from Lyakhovsky *et al.*[2]). The latest analysis of laboratory acoustic emission and stress-strain data, and their comparison to theoretical modelling, confirms this assumption (Liu *et al.*[45]). Increasing the additional modulus γ, from zero for linear-elastic damage-free material to its maximum value at the critical damage amplifies the material non-linearity with damage accumulation. Lyakhovsky *et al.*[2] suggest that the damage rate equation has different forms for weakening and for healing. These are, respectively:

$$\frac{d\alpha}{dt} = \begin{cases} C_d I_2(\xi - \xi_0), & \text{for } \xi \ge \xi_0 \\ C_1 \exp(\alpha / C_2) \cdot I_2(\xi - \xi_0), & \text{for } \xi \le \xi_0 \end{cases} \qquad [4]$$

Both equations include a material property ξ_0 that indicates the critical diagonality transition stage from strengthening to degradation. Agnon and Lyakhovsky[5] and Lyakhovsky *et al.*[2] related this parameter to the angle of internal friction by considering the critical shear stress for Mohr-Coulomb sliding. They received ξ_0=-0.8 for typical ratios of elastic moduli for damage-free material $\lambda/\mu \sim 1$ (Poisson's ratio of 0.25) and internal friction angle $\varphi \sim 40$ (Equation [37] and Figure 3 from Lyakhovsky *et al.*[2]). This value varies little for different rocks with Poisson ratios between 0.2 and 0.3 and is used for the following numerical simulations. The coefficient C_d is the damage rate constant, which defines the time needed to achieve failure after the onset of damage at $\xi=\xi_0$. C_d is assumed to be a material property and its value has been estimated to vary from 0.5 to 5 s^{-1} for different rocks tested at more than 20 MPa confining pressure and room temperature (Lyakhovsky *et al.*[2]). This parameter certainly depends on temperature and chemical environment, two factors that are not treated in this paper. It also might be pressure-

dependent, especially at low confining pressures. Making the damage rate for healing proportional to the exponent of the current level of a damage level (α) gives logarithmic-in-time material recovery that mimics the logarithmic-in-time increase of the static friction with the duration of stationary contact, as reported by Dieterich[46] and followers. This allows relating the constants C_1 and C_2 which describe the rate of healing, to the coefficients of the experimental static friction law [Lyakhovsky *et al.*[2]].

When deformation in some region achieves a threshold state ($\xi=\xi_0$), the damage starts to increase, weakening the material element. The weakening ends when the damage level becomes critical and stress-drop occurs (see Equations [14], [15] and Figure 1 of Lyakhovsky *et al.*[2] for the relation between the critical damage α_{cr} and strain diagonality ξ). The brittle failure leads to an increase of non-reversible plastic deformation, corresponding to the non-reversible slip in models that approximate the fault structure as a plane. During failure, the local deviatoric stresses of the destroyed element drop to zero, keeping only the confining component. This is supported by laboratory experiments (e.g., Brune *et al.*[47]), theoretical models (e.g., Heaton[48], Mora and Place[49], Andrews and Ben-Zion[50]) and a variety of geophysical observations (see Ben-Zion and Andrews[51], for a summary). After failure, the stress conditions in the post-failure region favour healing, which may last until close to the next failure event. The duration of the cycling between previous and subsequent failure depends on the rate of loading and material recovery.

The actual dynamic process, wherein waves are generated by the stress drop, is not simulated here. However, a quasi-dynamic procedure is applied to simulate a rupture front propagation. This is accomplished by recalculating the stress field after each stress drop in every element involved in the rupture process, and by incorporating dynamic weakening of material; the latter is achieved by reducing the critical value of the damage level, α_{cr}, to $\alpha_{dynamic}$:

$$\alpha_{dynamic} = \alpha_{cr} - \sqrt{\tau_a \frac{d\alpha}{dt}} \qquad [5]$$

where τ_a is material parameter. The condition $\alpha=\alpha_{cr}$ means that the material does not support any static load. Mathematically this criterion corresponds to a loss of convexity of the elastic energy U (Equation [2]) or to a zero elastic modulus in the 1-D case. In reality, that condition can be achieved only if damage increase is infinitesimally slow. Damage increase at a finite rate causes amplification of elastic waves. Using the linear relation between elastic moduli and damage level, the characteristic time of this amplification is found to be

$$(\alpha_{cr} - \alpha)^2 / \frac{d\alpha}{dt}.$$

On the other hand, waves are attenuated with characteristic time τ_a, which is related to the quality factor of the medium ($\tau_a \sim Q/f$, where f is a frequency) (Aki and Richards[53]). While the amplification makes the system dynamically unstable, the attenuation brings the system back to the stable regime. The dynamic instability occurs when these processes have balanced effect, or when α is slightly below the α_{cr} corrected after the rate of damage increase and attenuation. A detailed derivation of Equation [5] and its consequences are given in Agnon *et al.*[55,58].

Numerical method

Our three-dimensional numerical simulations use the Fast Lagrangian Analysis of Continua (FLAC) algorithm (Cundall and Board[59], Cundall[60], Poliakov *et al.*[61]). The formulation is explicit-in-time, using an updated Lagrangian scheme to provide the capability for large strains. The FLAC algorithm is believed to offer advantages over conventional finite element schemes in case where material instability occurs. Physical instability is modelled without numerical instability if inertial terms are included in the equilibrium equations. The general procedure basically involves solving a force balance equation for each grid point in the body

$$\frac{\partial v_i}{\partial t} = \frac{F_i}{m} \qquad [6]$$

where v_i and F_i are the velocity and the force applied to a node of mass m. The solution of the equations of motion provides velocities at each grid point, which are used to calculate element strains. These strains, when substituted into the linear or non-linear constitutive relation, provide element stresses and then forces acting at the element faces. These forces recalculated to the grid nodes are the necessary input for the solution of the equation of motion on the next cycle of calculation.

The computational mesh consists of tetrahedral elements. The four linear element shape function L_k (k = 1,4 –number of element node) are

$$L_k = a_k + b_k x_1 + c_k x_2 + d_k x_3 \qquad [7]$$

where a_k, b_k, c_k, d_k are constants and (x_1, x_2, x_3) are coordinates inside the element. These shape functions are used to linearly interpolate the nodal velocities ($V_i^{(k)}$) within each element and enables the calculation of the strain increments $D\varepsilon_{ij}$

$$D\varepsilon_{ij} = Dt \cdot \sum_{k=1}^{4} \left(V_i^{(k)} \frac{\partial L_k}{\partial x_j} + V_j^{(k)} \frac{\partial L_k}{\partial x_i} \right). \qquad [8]$$

After the elastic strains are thus calculated the stress tensor is computed using the constitutive relation [2], which in our case also includes the level of damage in the specific element. The nodal forces are now vector sums of one-third of the forces acting on all faces adjacent to the node:

$$F_i = \sum_{\text{faces}} \frac{1}{3} \sigma_{ij} n_j + m g_i \qquad [9]$$

where n_j is a normal vector to the face, m is one-fourth of the masses of elements adjacent to the node, and g_i is the gravity acceleration vector. Once the forces are known, new velocities are computed by integrating [6] over a given time step:

$$V_i^{(n+1)}(t + Dt) = V_i^{(n)}(t) + \left[F_i^{(n)} - \chi \left| F_i^{(n)} \right| \text{sign}\left(V_i^{(n)} \right) \right] \frac{Dt}{m_{\text{inert}}} \qquad [10]$$

During the integration, the previously calculated force ($F_i^{(n)}$) is damped. The damping term is proportional to the acceleration (out-of-balance) force with damping factor $0<\chi<1$ and has a sign opposite to that of the velocity. It accounts for the energy dissipation and for the attenuation if the elastic waves in the simulated area. This term vanishes if the system is in equilibrium and provides a convergence of numerical procedure to a steady-state solution. Following Poliakov *et al.*[61] we use 'inertial' mass in [10] instead of 'gravity' mass in [6] to allow adaptive time scaling. The time step, which provide stability of the numerical scheme is:

$$Dt = \frac{1}{2}\frac{Dx}{V_p} \qquad [11]$$

where Δx is a minimal distance between grid points and V_p is maximum possible seismic velocity in the material. Introducing density scale factor ($m_{incr}=D_s\ m$) we decrease V_p as square root of D_s and proportionally increase the time step without any numerical artifacts. This certainly could be done only if the system is close to equilibrium (out-of-balance force approaches to zero). This adaptive procedure, starting with D_s=1, automatically increases D_s if the system is in a steady-state regime, or brings it back to '1', if the solution deviates from static.

The damage level (α) for each element is calculated for every numerical cycle according to Equation [4] with time step defined by an adaptive procedure. If the damage in one element reaches its critical level, a stress drop occurs and some plastic strain is accumulated in this specific element. The stress recalculation is repeated until full equilibration. Next we search for other elements in which the damage is above critical level corrected after the dynamic weakening [5]. If such elements exist, they can not further keep the stress, and it should be dropped also. Finally, the list of elements involved in the failure process and accumulated plastic strain components are recorded together with the values of the stress drop for the calculation of the seismic source parameters.

The damage rheology and the above-described numerical scheme is the central engine of the Integrated Model described in (Ilchev and Lyakhovsky, this issue). In the following sections we present two examples of simulations which demonstrate the functionality of the damage rheology and the accuracy of numerical calculations.

Geometry of the process zone around mode-I crack

Consider a mode-I crack embedded in an infinite elastic solid governed by damage rheology. Suppose that the crack lies in a horizontal plane and propagates in its own direction (Figure 1). The formulation of the problem indicates a mirror symmetry with respect to the crack plane and with respect to the vertical line splitting the crack into two halves. This symmetry dictates a two-dimensional formulation of the problem. The simulated area is bounded by two free-slip lines (see Figure 1). The right edge of the simulated area is placed far enough from the crack tip (maximum crack length is 0.3 of the area size) and

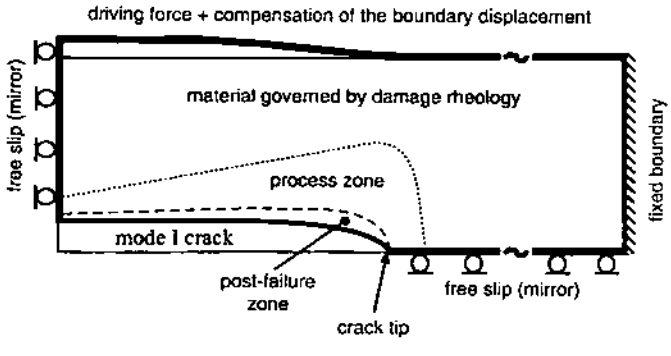

Figure 1. The problem set up for numerical simulation of crack propagation. The variable force vector, F_i, applied to each node at the top boundary, corresponds to the constant traction force, F_d, applied infinitely far from the simulated region

therefore the zero displacement boundary condition has a negligibly small effect on the stress distribution inside.

The setting of prescribed values (either forces or displacements) on the upper boundary of the simulated area is not quite straightforward. The problem stems from the conflict between the character of the loading (in this case it should be a constant driving force applied at infinity) and the finite size of the simulated area. The model boundary will have to be a virtual surface which separates the relatively small modelled area from the surrounding infinite material. The way one sets the conditions on this virtual boundary must be compatible with the driving force which is physically applied at infinity. In a sense the physical boundary conditions at infinity must induce the model boundary conditions for the simulated area. But this is not the end of the problems with the boundary conditions for damage rheology modelling of non-linear material response to loading. Every time step of the simulation brings a change of the state of damage in the simulated area while the material beyond the model boundary is still assumed to be a linear elastic medium. This results in additional contact interactions along the boundary of the simulated area. The effect of these contact interactions cannot be calculated *a priori* and needs to be re-evaluated at every time step of the simulation. There are two ways of achieving this: one can either use the additional forces at the boundary nodes to calculate the corresponding additional displacements or use the additional displacements to update the boundary forces. When we speak of 'additional forces' we mean the difference between the force in a boundary node as calculated by the FLAC algorithm at the current time-step and the corresponding reference value of the force as specified in the initial conditions. Clearly the engine to facilitate the evolution of the boundary conditions due to the progressive damage (or healing) in the simulated area must be a boundary forces to boundary displacements convertor of the boundary-element type. The general principles of the integration of a damage rheology model with a boundary-element shell are discussed in (Ilchev and Lyakhovsky, submitted to this conference).

In the simulation of the process zone around a mode-I crack the time and space variable force vector corresponding to the constant uniform traction applied infinitely far from the simulated area is calculated according to the linear elasticity equation.

$$F_i = F_d + \frac{\mu_0}{\pi(1-\nu)}\int_{-\infty}^{\infty}\frac{\partial u_i}{\partial x}\frac{d\zeta}{x-\zeta} \qquad [12]$$

where F_d is a driving force per unit area applied at infinity; F_i and u_i are boundary force and displacement, respectively; μ_0 is shear modulus and ν is Poisson ratio of the damage-free material. The fully three-dimensional formulation of the compensation after outer space deformation is discussed by Ilchev and Lyakhovsky (this issue).

The crack starts to grow from a small notch (0.03 of the area length) in a damage-free material. Stress concentration around the crack tip results in a build up of a process zone or a zone where the damage is non-zero (α>0). When the damage in front of the crack tip achieves its critical value, the crack length increases and previously destroyed elements form a crack boundary. Thus, a post-failure zone (a zone where plastic strain is accumulated and the material effectively behaves as a gouge zone governed by healing) surrounds the crack. The velocity of quasi-static, damage-

controlled crack propagation depends on the rate of damage increase. The time scale of the damage increase, t_d, is defined by the kinetics of the damage process:

$$t_d = \left(\frac{\mu_o}{F_d}\right)^2 \frac{1}{c_d} \qquad [13]$$

Results of numerical simulation (Figure 2) show the self-similar growth of the damage zone as it was supposed for the quasi-static crack. The material properties used in this and other simulations are: ξ_0=-0.8, C_d=1 s^{-1}, C_1=10^{-8} s^{-1}, C_2=0.05, μ_0=λ (Poisson ratio 0.25), μ_0/F_d=10^{-3}. According to [13] the time scale, t_d, is equal to 10^6 s. These simulations are carried out under the limit, where the relaxation time is much shorter than the damage time scale (t_d>>τ_a). Hence, self-similarity for quasi-static crack growth is preserved. The proportional increase of the process zone with crack length indicates that the damage rate around the propagating crack is self-similar and should fit the power law with some index m and a dimensional coefficient B:

$$t_d = \frac{d\alpha}{dt} = B.L^m \qquad [14]$$

Equation [14], together with the equation for the dynamic weakening [5], allows defining the upper boundary of the crack length, L_{cr}, for a crack propagating in the quasi-static self-similar regime described by equations:

$$L_{cr} = \left(\frac{B\tau_a}{t_d}\right)^{-\frac{1}{m}} \qquad [15]$$

Substituting [15] into [14] and then into [5] gives zero critical damage (α_{cr}=0) for the crack length equal to L_{cr}. Consequently, a process zone is not created around the crack tip, the quasi-static regime is impossible and the crack propagates in the dynamic regime governed by an elasto-dynamic equation e.g., Freund[52]. This transition is shown in Figure 3 for the simulated crack growth with τ_a=30•t_d. All other material and geometrical parameters are the same as in the quasi-static case. The dynamic weakening starts to decrease the critical damage value and crack growth accelerates. This acceleration could not be related to the proximity of the boundary on the right, because it has an opposite effect slowing down much longer cracks. When crack velocity approaches the speed of elastic waves, the crack growth ceases to be controlled by the damage process. The process zone around the crack changes its shape due to the dynamic weakening (Figure 3). Prior to the significant reduction in critical damage (Figure 3a), it is similar to that around a quasi-static crack (Figure 2a). Further reduction of the critical damage decreases the size of the process zone (Figure 3b). The slope of the outer boundary of the process zone behind the crack tip is much lower and some of the internal iso-damage lines have negative slope. This tendency is amplified with further crack acceleration (Figure 3c), reducing the process zone size to zero. Thus, the process zone of the dynamically propagating crack is very small, or does not exist at all.

Propagation path under mixed mode loading

A tensile fracture propagates in its own direction only under driving tensional (or compressional) force perpendicular to the crack plane. Laboratory experiments and theory suggest that even minor component of a mode-II loading will cause deviation from the in-plane propagation and breakdown of the crack front (e.g., Erdogan and Sih[54], Cotterell and Rice[56], Cooke and Pollard[57]). There are different theoretical criteria predicting the propagation direction of mixed mode I+II cracks (see Cooke and Pollard[57] for review), which can hardly be distinguished experimentally. Here we investigate a simplified case where a pre-existing crack is tensioned by force acting in the direction with a crack angle β between crack plane and direction of the force. The Erdogan and Sih[54] maximum tangential stress criterion predicts a fracture angle φ which varies between 0° and 71° according to the crack angle:

$$\sin(\varphi) + (3.\cos(\varphi) - 1).\cot(\beta) = 0 \qquad [16]$$

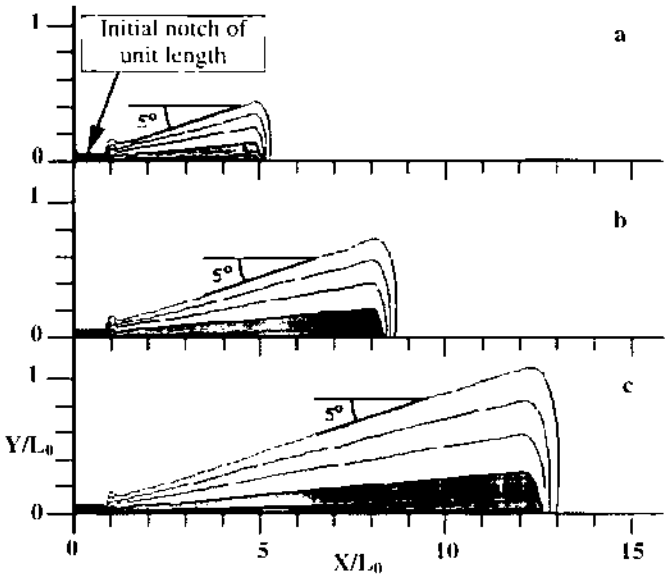

Figure 2. The process zone for three different stages of quasi-static crack growth has self-similar geometry with a constant ~5° slope of the outer boundary. Here and in Figure 3 the step between contour levels is equal 0.1

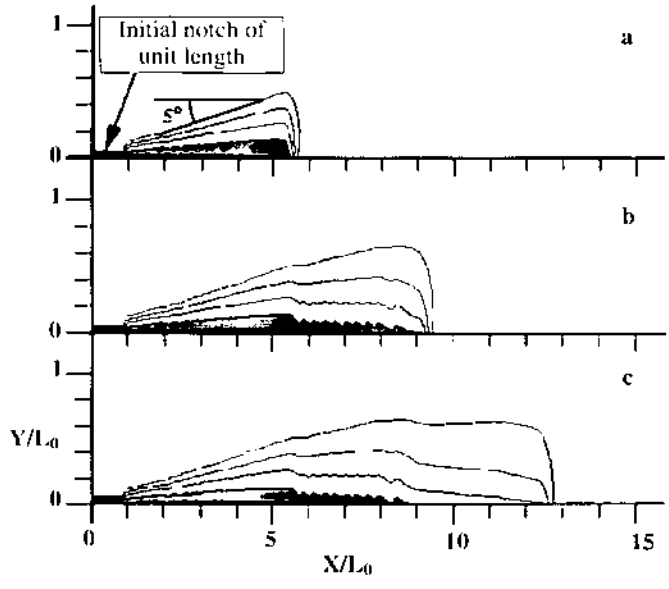

Figure 3. The process zone around the crack has the same geometry until the dynamic weakening is negligible (a). The size of the process zone increases much more slowly when the dynamic weakening becomes important (b), and even decreases at the crack acceleration stage (c)

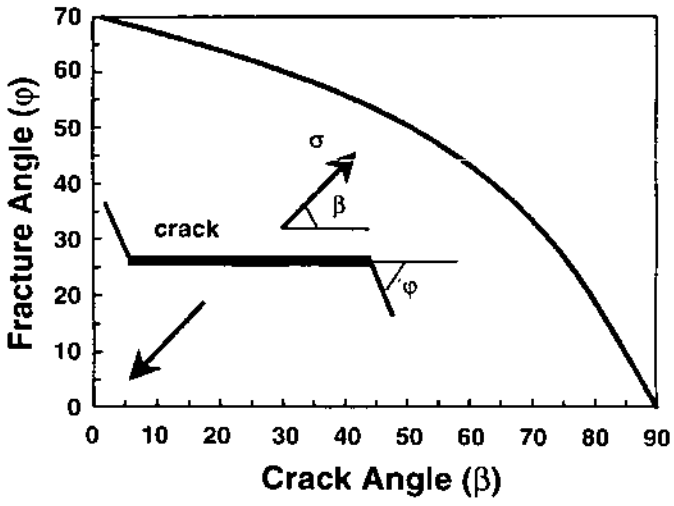

Figure 4. Theoretically predicted and experimentally confirmed relation (Erdogan and Sih[54]) between crack angle b and fracture angle j [equation 16]

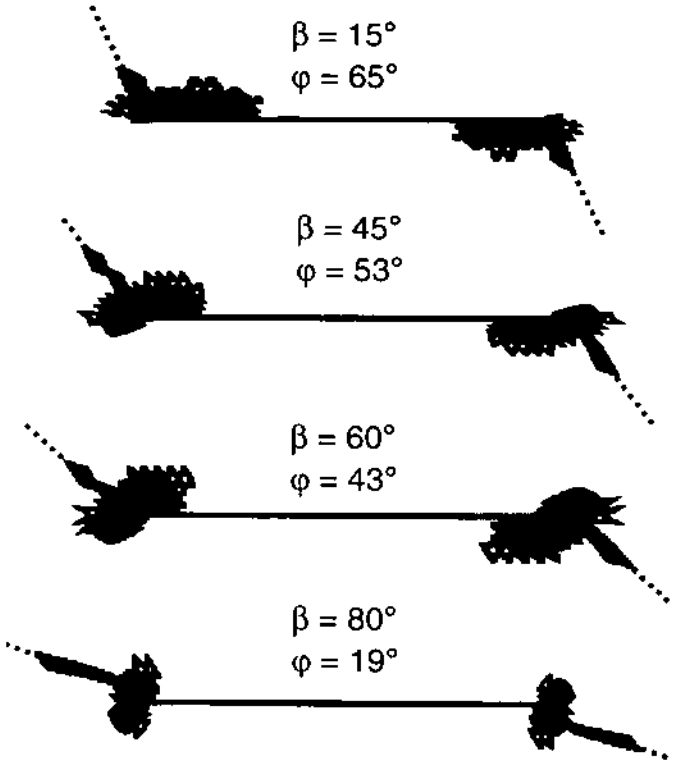

Figure 5. Geometry of the damage zones around the narrow pre-existing fracture subjected to out-of plane load with crack angle b=15°, 45°, 60°, and 80°. Propagation path of highly destroyed zone perfectly fits the theoretically predicted direction (dotted lines)

as shown in Figure 4. The damage rheology model does not allow introducing pre-existing cracks in its current numerical formulation. Moreover, the increasing damage removes any stress singularities making the solution regular everywhere. Thus, it is not obvious if the narrow pre-existing damage zone subjected to the oblique tension will propagate in direction compatible with those predicted by linear elastic fracture mechanics. The results of different runs with geometry of new created damage zone around pre-existing one are shown in Figure 5. The dotted lines represent the predicted orientation of crack propagation calculated using [16]. Under different orientations of the loading the new created high damaged zones fit well the predicted path, which confirm the ability of the damage rheology approach and accuracy of numerical calculations.

Conclusions

The damage rheology model outlined above is based on the fundamental principles of continuum mechanics and thermodynamics as well as on the observations of rock deformation. Its advantage over other crack propagation models is that it provides the time and spatial scaling of the fracture process and reproduces the main features of sub-critical crack growth under constant and cycling loads, including transition between quasi-static and a dynamic regime. The results of numerical analyses of mode I crack growth show that the geometry of the process zone around a quasi-static crack has a self-similar shape identical to the universal scaling of linear fracture mechanics. The dynamic weakening decreases the critical damage value and leads to acceleration of the crack growth. When dynamic weakening reduces the critical damage to zero, the process zone vanishes and the crack propagates in a dynamic regime. Under mixed mode I+II loading the model correctly predicts the kink angle of the fracture front breakdown.

References

1. KACHANOV, L.M. *Introduction to continuum damage mechanics*, Martinus Nijhoff Publishers, 1986. p. 135.
2. LYAKHOVSKY, V., BEN-ZION, Y., and AGNON, A.,Distributed damage, faulting, and friction, *J. Geophys. Res.*, 102, 1997a. pp. 27,635–27,649.
3. LYAKHOVSKY, V., RECHES, Z., WEINBERGER, R., and SCOTT, T.E. Non-linear elastic behavior of damaged rocks, *Geophys. J. Int.*, 130, 1997b. pp. 157–166.
4. BYERLEE, J.D. Friction of rocks, *Pure and Appl. Geophys.* 116, 1978. pp. 615–626.
5. AGNON, A. and LYAKHOVSKY, V. Damage distribution and localization during dyke intrusion, in *The Physics and Chemistry of Dykes*, edited by G. Baer and A. Heimann, Balkema, Rotterdam, 1995. pp. 65–78.
6. ANDERSON, E.M. *The dynamics of faulting*, 183 pp., Oliver and Boyd, London, 1951.
7. CHINNERY, M.A. Secondary faulting, 1. Theoretical aspects, 2. Geological aspects. *Canad. J. Earth Sci.*, 3, 1966. pp. 163–190.
8. SCHOLZ, C.H. *The mechanics of earthquakes and faulting*. Cambridge University, England. 1990. p. 439.
9. RUBIN, A.M. Propagation of magma filled cracks. *Ann. Rev. Earth Planet. Sci.* 8, 1995a. pp. 287–336.
10. Rubin, A.M. Why geologists should avoid using 'fracture toughness' (at least for dikes), in *The Physics and Chemistry of Dykes*, edited by G. Baer and A. Heimann, Balkema, Rotterdam, 1995b. pp. 53–65.
11. DELANEY, P.T., POLLARD, D.D., ZIONY, J.I., and McKEE, E.H. Field relations between dikes and joints: emplacement processes and paleostress analysis. *J. Geophys. Res.*, 91, 1986. pp. 4920–4938.

12. BAER, G. Mechanisms of dike propagation in layered rocks and in massive, porous sedimentary rocks. *J. Geophys. Res.*, 96, 1991. pp. 11911–11929.
13. WEINBERGER, R., BAER, G., SHAMIR, G., and AGNON, A. Deformation bands associated with dyke propagation in porous sandstone, Makhtesh Ramon, Israel, in *The Physics and Chemistry of Dykes*, edited by G. Baer and A. Heimann, Balkema, Rotterdam, 1995. pp. 95–115.
14. HOEK, J.D. Dyke propagation and arrest in Proterozoic tholeiitic dyke swarms, Vestfold Hills, East Antarctica, in *The Physics and Chemistry of Dykes*, edited by G. Baer and A. Heimann, Balkema, Rotterdam, 1995. pp. 79–95.
15. SCHOLZ, C.H., DAWERS, N.H., YU, J.-Z., ANDERS, M.H., and COWIE, P.A. Fault growth and fault scaling laws: Preliminary results. *J. Geophys. Res.*, 98, 1993. pp. 21951–21961.
16. VERMILYE, J.M. and SCHOLZ, C.H. The process zone: A microstructural view of fault growth. *J. Geophys. Res.*, 103, 1998. pp. 12,223–12,236.
17. BAZANT, Z.P. and KAZEMI, M.T. Determination of fracture energy, process zone length and brittleness number from size effect, with application to rock and concrete. *Int. J. Fracture*, 44: 1990. pp. 111–131.
18. SINCLAIR, G.B. and CHAMBERS, A.E. Strength size effect and fracture mechanics: what does the physical evidence say? *Eng. Fract. Mech.*, 26, 1987. pp. 279–310.
19. HATTON, C.G., MAIN, I.G., and MEREDITH, P.G. Non-universal scaling of fracture length and opening displacement, *Nature*, 367, 1994. pp. 160–162.
20. RENSHAW, C.E. and PARK, J.C. Effect of mechanical interactions on the scaling of fracture length and aperture. *Nature*, 386, 1997. pp. 482–484.
21. NISHIHARA, M. Stress-strain relation of rocks. *Doshisha Eng. Rev.*, 8, 1957. pp. 32–55.
22. ZOBACK, M.D. and BYERLEE, J.D. The effect of microcrack dilatancy on the permeability of Westerly granite. *J. Geophys. Res.*, 80-B, 1975. pp. 752–755.
23. SCHOCK, R.N. The response of rocks to large stresses. in D.L. Roddy, R.O. Pepin, and R.B. Merrill (editors). *Impact and explosion cratering*, Pergamon Press, New York, NY, 1977. pp. 657-688.
24. SCHOCK, R.N. and LOUIS, H. Strain behavior of a granite and a graywacke sandstone in tension. *J. Geophys. Res.*, 87, 1982. pp. 7817–7823.
25. LOCKNER, D.A. and BYERLEE, J.D. Development of fracture planes during creep in granite. in: *2nd Conference on Acoustic Emission/ Microseismic Activity in Geological Structures and Materials*, Trans-Tech. Publications, Clausthal-Zellerfeld, Germany, 1980. pp. 1–25.
26. ALM, O., JAKTLUND, L.L., and KOU, S. The influence of microcrack density on the elastic and fracture mechanical properties of Stripa granite. *Phys. Earth. Planet. Inter.*, 40, 1985. pp. 161–179.
27. RECHES, Z. and LOCKNER, D.A. Nucleation and growth of faults in brittle rocks. *J. Geophys. Res.*, 99, 1994. pp. 18159–18173.
28. WEINBERGER, R., RECHES, Z., SCOTT, T.S., and EIDELMAN, A. Tensile properties of rocks in four-point beam tests under confining pressure, in: *Proceedings First North American Rock Mechanics Symposium*, Austin, Texas, 1994. pp. 435–442.
29. PESTMAN, B.J. and MUNSTER, J.G. An acoustic emission study of damage development and stress—memory effects in sandstone. *Int. J. Rock Mech. Min. Sci.*, 33, 1996. pp. 585–593.
30. LOCKNER, D.A., BYERLEE, J.D., KUKSENKO, V., PONOMAREV, A., and SIDORIN, A. Observations of quasi-static fault growth from acoustic emission. In: *Fault mechanics and transport properties of rocks*. International geophysics series, v. 51, B. Evans and T.-F. Wong (eds.), Academic Press, 1992. pp. 3–31.
31. YUKUTAKE, H. Fracturing process of granite inferred from measurements of spatial and temporal variations in velocity during triaxial deformation. *J. Geophys. Res.*, 94, 1989. pp. 15639–15651.
32. LOCKNER, D.A., BYERLEE, J.D., KUKSENKO, V., PONOMAREV, A., and SIDORIN, A. Quasi-static fault growth and shear fracture energy in granite. *Nature*, 350, 1991. pp. 39–42.
33. DUGDALE, D.S. Yielding of steel sheets containing slits. *J. Mech. Phys. Solids*, 8, 1960. pp. 100–104.
34. BARENBLATT, G.I. Mathematical theory of equilibrium cracks in brittle fracture. *Acv. Appl. Mech.*, 7, 1962. pp. 55–129.
35. BARENBLATT, G.I. *Scaling, self-similarity, and intermediate asymptotics*, Cambridge Univ. Press, 1996.
36. IDA, Y. Cohesive force across the tip of longitudinal shear crack and Griffith's specific surface energy. *J. Geophys. Res.*, 77, 1972. pp. 3796–3805.
37. PALMER, A.C. and RICE, J.R. The growth of slip surfaces in the progressive failure of over-consolidated clay. *Proc. Roy. Soc. London*, Ser. A, 332, 1973. pp. 527–558.
38. RUBIN, A.M. Tensile fracture of rock at high confining pressure: Implications for dike propagation, *J. Geophys. Res.* 98, 1993. pp. 15,919–15,935.
39. WILLEMSE, E.J.M. and POLLARD, D.D. On the orientation and patterns of wing cracks and solution surfaces at the tips of a sliding flaw or fault. *J. Geophys. Res.*, 103, 1998. pp. 2427–2438.
40. BAZANT, Z.P. and CEDOLIN, L. *Stability of structures*. Elastic, Inelastic, fracture and damage theories. Oxford University Press, 1991. p. 984.
41. HUANG, W-L., KUNIN, B., and CHUDNOVSKY, A. Kinematics of damage zone accompanying curved crack. *Int. J. Fracture*, 50, 1991. pp. 143–152.
42. CHAI, H. Observation of deformation and damage at the tip of cracks in adhesive bonds loaded in shear and assessment of a criterion for fracture. *Int. J. Fracture*, 60, 1993. pp. 311–326.
43. ZIETLOW, W.K. and LABUZ, J.F. Measurements of the intrinsic process zone in rock using acoustic emission, *Int. J. Rock Mech. Min. Sci.*, 35, 1998. pp. 291–299.
44. MURNAGHAN, F.D. *Finite deformation of an elastic solid*, John Wiley, Chapman, New York, 1951.
45. LIU, Y., LYAKHOVSKY V., BEN-ZION, Y., and LOCKNER, D. Analysis of acoustic emission and

stress-strain laboratory data with a damage rheology model. Fall AGU meeting. 1999.

46. DIETERICH, J.H. Time-dependent friction in rocks. *J. Geophys. Res.*, 77. 1972. pp. 3690–3697.
47. BRUNE, J.N., BROWN, S., and JOHNSON, P.A. Rupture mechanism and interface separation in foam rubber model of earthquakes: a possible solution to the heat flow paradox and the paradox of large overthrusts, *Tectonophysics*, 218, 1993. pp. 59–67.
48. HEATON, T.H. Evidence for and implications of the self-healing pulses of slip in earthquake rupture, *Phys. Earth Planet. Int.*, 64, 1990. pp. 1–20.
49. MORA, P. and PLACE, D. Simulation of the frictional stick-slip instability, *Pure Appl. Geophys.* 143, 1994. pp. 61–87.
50. ANDREWS, D.J. and BEN-ZION, Y. Wrinkle-like Slip Pulse on a Fault Between Different Materials, *J. Geophys. Res.*, 102, 1997. pp. 553–571.
51. BEN-ZION, Y. and ANDREWS, D.J. Properties and implications of dynamic rupture along a material interface, *Bull. Seismol. Soc. Amer.*, 88, 1998. pp. 1085–1094.
52. FREUND, L.B. *Dynamic fracture mechanics*, Cambridge University Press. 1990. p. 563.
53. AKI, K. and RICHARDS, P.G. *Quantitative seismology, theory and methods*. W.H. Freeman, San Francisco. 1980.
54. ERDOGAN, F. and SIH, On the crack extension in plates under plane loading and transverse shear. *Trans. Am. Soc. Mech. Engng.* 85, 1963. pp. 519–527.
55. AGNON, A., LYAKHOVSKY, V., and BEN-ZION, Y. Localization of distributed damage and strain to stick-slip faults. In: *Localization phenomena and dynamics of brittle and granular systems*, Columbia University, NY, C.H. Scholz (ed.), 1997. pp. 33-39.
56. COTTERELL, B. and RICE, J.R. Slightly curved or kinked cracks, *Int. J. Fract.* 16, 1980. pp. 155–169.
57. COOKE, M.L. and POLLARD, D.D. Fracture propagation paths under mixed mode loading within rectangular blocks of polymethyl methacrylate. *J. Geophys. Res.*, 101, 1996. pp. 3387–3400.
58. AGNON, A., LYAKHOVSKY, V., and BEN-ZION, Y. (in preparation). A continuum approach to rock friction. 2000.
59. CUNDALL, P. A. and M. BOARD. A microcomputer program for modeling large-strain plasticity problems, in Numerical Methods in Geomechanics, *Proceedings of 6th International Conference on Numerical Methods in Geomechanics, Innsbruck*, (edited by C. Swoboda), R.A. Balkhema, Brookfield, Vt. 1988. pp. 2101–2108.
60. CUNDALL, P.A. Numerical experiments on localization in frictional materials. *Ign. Arch.*, 59:1989 pp. 148–159.
61. POLIAKOV A., CUNDALL P., PODLADCHIKOV YU., and LYAKHOVSKY V. An explicit inertial method for the simulation of viscoelastic flow: An evaluation of elastic effects on diapiric flow in two and three layer models. *Proceedings of NATO Advanced Study Institute on Dynamic Modeling and Flow in the Earth and Planets*. In: D.B. Stone and S.K. Runcorn (eds.), Flow and Creep in the Solar system: Observations, Modeling and Theory, Kluwerr, Holland, 1993. pp. 175–195.